

# Relativistic Spectroscopy of Plasma Embedded Li-like Systems with the Screening Effects in the Two-body Debye Potentials

<sup>1</sup>Madhulita Das, <sup>2</sup>B. K. Sahoo and <sup>1</sup>Sourav Pal

<sup>1</sup>National Chemical Laboratory, Pune - 411008, India and

<sup>2</sup>Theoretical Physics Division, Physical Research Laboratory, Navrangpura, Ahmedabad - 380009, India

The spectroscopic properties of Li atom and Li-like Ca and Ti ions in the plasma environment are investigated using a relativistic coupled-cluster (RCC) method. Assuming the plasma is of low density and very hot, we consider the Debye model with two approximations by accounting the screening effects: (i) in the nuclear potential alone and (ii) in both the nuclear and the electron-electron interaction potentials. First, the calculations for the energies and the lifetimes of the atomic states are carried out for the plasma free systems in order to check their accuracies following which they are investigated in the plasma environment. It is observed that screenings in the electron-electron interaction potentials stabilize the systems more than the case when the screenings present only in the nuclear potential. Similarly, the earlier predicted blue and red shifts in the  $\Delta n = 0$  and  $\Delta n \neq 0$  transition lines (with the principal quantum number  $n$ ) of the Li-like ions change significantly in the case (ii) approximation. The level-crossings among the energy levels are observed for the large screening effects which seem to be prominent in the states of higher orbital angular momentum. The lifetimes of many low-lying states and the relative line-intensities of the allowed transitions are estimated considering different plasma screening strengths.

PACS numbers:

## I. INTRODUCTION

The knowledge of spectral properties of the atomic systems immersed in the plasma environment is an important tool for plasma diagnostic processes and also have a wide range of applications in many research fields such as in the astrophysics, inertial confinement fusion (ICF), magnetic confinement fusion, laser-matter interaction, X-ray lasers, etc. [1–5]. Usually, the spectral properties of the plasma embedded atomic systems change considerably in comparison to the isolated systems due to the presence of other charged particles in the plasma confinement. The radiations coming out from the plasma embedded atomic systems, through various excitations or ionization processes, play crucial roles for providing insights of the physical phenomenon happening inside the plasma. It has been found from the laser-plasma experiments that the red shifts of the atomic emission lines are of the order of 3.7 eV [6, 7]. The detailed understanding of such findings requires a proper characterization of the atomic spectral lines emitted from the systems. Therefore, the theoretical investigation of the atomic spectroscopy in the hot and dense plasma has become an exciting field of research.

The plasma environment mostly consists of ions and free electrons, which introduce screening effects in the Coulomb potentials of the embedded atomic systems. Thus, the atomic electrons are highly influenced by the external electromagnetic fields compelling the atomic long range electrostatic potentials to act as short range screened potentials. In general, it is computationally difficult to take complete interactions into the calculations. However, the theoretical studies of the properties in these atomic systems are conveniently carried out by defining suitable model potentials in the atomic Hamilto-

nian by estimating the screening effects depending upon the strength of the plasma. The strength of the plasma is defined by a coupling parameter ( $\Gamma$ ) that measures the interactions between the particles inside the plasma environment. Debye model [8] is the most conventional approach used for studying atomic spectroscopy in low density and high temperature plasma (weakly coupled plasma; i.e  $\Gamma < 1$ ).

The phenomenon of reduction of ionization potential (IP) of an atom or an ion in the plasma environment is known as ionization potential depression (IPD) [9–12]. Accurate determination of this quantity can infer many useful information such as equation of state of plasma, radiative opacity of stellar plasma, inertial confinement fusion plasma, etc. Recently, experimental studies by Hoarty *et al.* [13] and Ciricosta *et al.* [14] reveal the influence of hot and dense plasma environment in the atomic properties and the IPDs in the Al atom are reported. Thus, the atomic structure probes in plasma have attracted both the experimentalists and theoreticians to make further attempt in yielding more accurate spectroscopic data. Many calculations on H-like and He-like ions in the dense plasma environment have been performed [15–18] for their simpler structures, but only a handful number of theoretical investigations are available for Li-like systems [19]. Nonetheless, there have been many emission spectra observed both in the astrophysical and the laboratory plasma corresponding to high nuclear charge [20–30]. For reliable identifications of these spectral lines and to comprehend better about the underlying physics of their origin, it is necessary to employ more accurate methods that can include both the relativistic and electron correlation effects appropriately in the theoretical analysis of the atomic spectral properties.

The primary thrust of the present work is to study

theoretically the effects of the plasma screenings in the spectroscopy of the highly ionized Ca XVIII and Ti XX ions (Li-like) and compare against the neutral Li atom. These ions are commonly used in the laser-plasma experiments [31, 32] and are of particular interest for the astrophysical-plasma studies [33]. Before evaluating the atomic properties in the plasma environment, we determine the IPs and the lifetimes of the atomic states in the plasma free case to compare them with the available experimental values to validate our calculations. Next, we introduce the screening effects in the nuclear potential using the Debye model and then add them in the electron-electron interaction potential in order to find out how the results differ in these two approximations. A relativistic coupled-cluster (RCC) many-body theory in the Fock-space representation has been employed for the calculations. We also give predicted values for the ratios of the line intensities among the atomic transitions.

The paper is organized as follows: In Sec. II, we introduce the screening models that are considered in the calculations of the atomic spectral properties and describe the employed RCC method briefly in Sec. III. We give the obtained results in Sec. IV along with their comparison with the other available results and discuss them before summarizing the work in Sec. V. Through out the paper, the units given for IP, excitation energies (EE), and fine structure (FS) splittings are in  $cm^{-1}$ , line strength ( $S$ ) and the Debye screening length ( $D$ ) are in atomic units (a.u.), transition rates ( $A$ ) are in  $sec^{-1}$  and lifetimes ( $\tau$ ) of the atomic states are in  $sec$ .

## II. DEBYE MODEL POTENTIALS

The atoms or ions embedded in a plasma are largely perturbed by the electromagnetic fields produced by the neighboring ions and the freely moving electrons of the plasma. It is almost impossible to account all the possible governing interactions among the particles in the exact determination of the structures of the atomic systems in such environment. Alternatively, the effectiveness of the interactions can be approximated using appropriate models to be able to explain the systems within reasonable accuracies for all the practical purposes. In a hot and low density plasma, the atomic systems get screened due to the penetration of the slowly moving free electrons of the plasma into the systems. Using the Poisson-Boltzmann equation, the effective potential under these conditions can be well approximated in the Debye model for a point

nuclear system as

$$V_{\text{eff}}(r_i) = -\frac{Z}{r_i}e^{-r_i/D} + \sum_{j \geq i}^{N_e} \frac{1}{r_{ij}}e^{-r_{ij}/D}$$

$$= V_{\text{nuc}}(r_i) + \sum_{j \geq i}^{N_e} V_{ee}(r_{ij}), \quad (1)$$

$$\text{where } D = \left[ \frac{k_B T_e}{4\pi(1+Z)n_e} \right]^{1/2} \quad (2)$$

is the Debye screening length,  $Z$  is the nuclear charge,  $N_e$  is the number of the electrons,  $k_B$  is the Boltzmann constant,  $T_e$  is the plasma temperature, and  $n_e$  is the plasma electron density.

In Eq. (1),  $V_{\text{nuc}}(r)$  represents the screened electron-nucleus potential whereas  $V_{ee}(r)$  is the screened electron-electron interaction potential. Due to computational difficulties, majority of the previous works on the spectroscopy study have considered the screenings only in  $V_{\text{nuc}}(r)$  where the electron-electron potential  $V_{ee}(r)$  is truncated at its first term of the exponential expansion for its dominant contribution [34]. We refer this approximation as ‘‘Model A’’ in this work. It is also important to take into account the screened effects in the electron-electron interactions for large plasma strengths to achieve more realistic results in the search for stability of the atomic structure in the plasma medium.

Instead of considering the point nucleus in the evaluation of  $V_{\text{nuc}}(r)$ , we use the Fermi-charge distribution to take into account the finite size of the nucleus by using the expression

$$V_{\text{nuc}}(r) = -\frac{Ze^{-r/D}}{\mathcal{N}r} \times$$

$$\begin{cases} \frac{1}{b} \left( \frac{3}{2} + \frac{a^2 \pi^2}{2b^2} - \frac{r^2}{2b^2} + \frac{3a^2}{b^2} P_2^+ \frac{6a^3}{b^2 r} (S_3 - P_3^+) \right) & \text{for } r \leq b \\ \frac{1}{r} \left( 1 + \frac{a62\pi^2}{b^2} - \frac{3a^2 r}{b^3} P_2^- + \frac{6a^3}{b63} (S_3 - P_3^-) \right) & \text{for } r > b \end{cases} \quad (3)$$

where the factors are

$$\mathcal{N} = 1 + \frac{a^2 \pi^2}{b^2} + \frac{6a^3}{b^3} S_3$$

$$\text{with } S_k = \sum_{l=1}^{\infty} \frac{(-1)^{l-1}}{l^k} e^{-lb/a}$$

$$\text{and } P_k^{\pm} = \sum_{l=1}^{\infty} \frac{(-1)^{l-1}}{l^k} e^{\pm l(r-b)/a}. \quad (4)$$

Here, the parameter  $b$  is known as the half-charge radius,  $a$  is related to the skin thickness of the nucleus. These two parameters are evaluated by

$$a = 2.3/4(\ln 3)$$

$$\text{and } b = \sqrt{\frac{5}{3} r_{\text{rms}}^2 - \frac{7}{3} a^2 \pi^2} \quad (5)$$

with the appropriate values of the root mean square radius,  $r_{rms}$ , of the nucleus.

To add the screening effects in the electron-electron interactions, we adopt the approximations considered in [35–39] as

$$V_{\text{eff}}(r_i) = V_{\text{nuc}}(r_i) + e^{-r_i/D} \sum_{j \geq i}^{N_e} \frac{1}{r_{ij}}. \quad (6)$$

This approximation is labeled as “Model B” in the present work.

### III. METHOD OF CALCULATIONS

We employ the one-valence electron attachment RCC method developed by us (e.g. see Refs. [40–42]) for carrying out calculations of the atomic wave functions in the considered systems which is briefly described below. The four-component Dirac-Hamiltonian along with the effective potentials that is used for the wave function calculations of the plasma embedded atomic systems is given by

$$H = \sum_{i=1}^{N_e} [c\vec{\alpha}_i \cdot \vec{p}_i + (\beta - 1)c^2 + V_{\text{eff}}(r_i)], \quad (7)$$

where  $N_e$  is number of electrons of the atomic system,  $\vec{\alpha}$  and  $\beta$  are the Dirac matrices and  $c$  is the velocity of light.

The ground states of the considered atomic systems have the  $[1s^2]$  closed-shell configuration and  $2s$  valence orbital. Also, many of the low-lying excited states in these systems have the same closed-shell configuration with an electron in one of the virtual orbitals instead of the  $2s$  orbital. To calculate these states, we express the atomic wave functions in our RCC method as

$$|\Psi_v\rangle = e^T \{e^{S_v}\} |\Phi_v\rangle, \quad (8)$$

where we define the reference state  $|\Phi_v\rangle$  by appending the appropriate valence orbital  $v$  of the corresponding state to the Dirac-Fock (DF) wave function of the  $[1s^2]$  configuration (denoted by  $|\Phi_0\rangle$ ). Here,  $T$  is the core excitation operator and  $\{S_v\}$  is the normal order excitation operator from core and valence to the virtual orbitals. Since the states have only one valence orbital in their configurations, the exponential form  $\{e^{S_v}\}$  naturally reduces to  $\{1 + S_v\}$  yielding the form

$$|\Psi_v\rangle = e^T \{1 + S_v\} |\Phi_v\rangle. \quad (9)$$

Considering the singles and doubles approximation in the RCC theory (CCSD method), the cluster operators  $T$  and  $S_v$  are defined by

$$\begin{aligned} T &= T_1 + T_2 \\ \text{and } S_v &= S_{1v} + S_{2v}. \end{aligned} \quad (10)$$

The amplitudes of these excitation operators are obtained by solving the following equations

$$\langle \Phi_0^K | \overline{H_N} | \Phi_0 \rangle = \delta_{K,0} \Delta E_{\text{corr}} \quad (11)$$

and

$$\langle \Phi_v^K | \overline{H_N} (1 + S_v) | \Phi_v \rangle = \langle \Phi_v^K | \delta_{K,v} + S_v | \Phi_v \rangle \Delta E_v, \quad (12)$$

where the values of the superscripts  $K (= 1, 2)$  represent the (singly and doubly) excited hole-particle states,  $\overline{H_N} = e^{-T} H_N e^T$  is the dressed part of the normal order Hamiltonian ( $H_N$ ).  $\Delta E_{\text{corr}}$  and  $\Delta E_v$  are the correlation energy and attachment energy (also equivalent to negative of the ionization potential (IP)) of the valence electron  $v$ , respectively.

The lifetime of a given state  $f$  is defined by the reciprocal of the total transition rate of that state due to all possible transition channels; i.e.

$$\tau_f = \frac{1}{\sum_{O,i} A_{f \rightarrow i}^O}, \quad (13)$$

for the transition rate  $A_{f \rightarrow i}^O$  due to a radiative operator  $O$ . The transition rates via various multipole channels are given by

$$A_{f \rightarrow i}^{\text{E1}} = \frac{2.02613 \times 10^{18}}{\lambda^3 (2J_f + 1)} S_{f \rightarrow i}^{\text{E1}} \quad (14)$$

$$A_{f \rightarrow i}^{\text{M1}} = \frac{2.69735 \times 10^{13}}{\lambda^3 (2J_f + 1)} S_{f \rightarrow i}^{\text{M1}} \quad (15)$$

and

$$A_{f \rightarrow i}^{\text{E2}} = \frac{1.11995 \times 10^{18}}{\lambda^5 (2J_f + 1)} S_{f \rightarrow i}^{\text{E2}}, \quad (16)$$

where  $\lambda$  is the wavelength ( $\text{\AA}$ ) and  $S_{f \rightarrow i}^O = |\langle f || O || i \rangle|^2$  is the line strength due to the corresponding transition operator  $O$ , and  $J_f$  is the total angular momentum of the  $f$  state. E1, M1, and E2 represent the electric dipole, magnetic dipole, and electric quadrupole transition channels respectively.

We have used Gaussian type of orbitals (GTOs) to construct the single particle orbitals. The large and small radial components of a Dirac orbital in this case are expressed by

$$P_\kappa(r) = \sum_\nu c_{\kappa,\nu}^P r^{l_\kappa} e^{-\zeta_\nu r^2} \quad (17)$$

and

$$Q_\kappa(r) = \sum_\nu c_{\kappa,\nu}^Q c_{\kappa,\nu}^P r^{l_\kappa} \left( \frac{d}{dr} + \frac{\kappa}{r} \right) e^{-\zeta_\nu r^2}, \quad (18)$$

respectively, where the summation over  $\nu$  stands for the total number of GTOs used in each orbital angular momentum ( $l_\kappa$ ) symmetry with the relativistic quantum number  $\kappa$ ,  $c_\nu^P$  and  $c_\nu^Q$  are the normalization constants and  $\zeta_\nu$  are the guessed parameters chosen suitably for different symmetries. In order to optimize the exponents, we use the even tempering condition

$$\zeta_\nu = \zeta_0 \eta^{\nu-1} \quad (19)$$

with two unknown parameters  $\zeta_0$  and  $\eta$ .

#### IV. RESULTS AND DISCUSSION

We first study the spectroscopic properties of plasma isolated atomic systems by considering  $D = \infty$  in Eq. (7). The rationale of carrying out these calculations are to verify the accuracies of our results by comparing them with the available experimental values. The obtained IPs and FS splittings of Li I, Ca XVIII and Ti XX from the CCSD method are given in Table I along with the recommended values from the national institute of science and technology (NIST) database [43]. We found good agreements between our results with the NIST data. Due to large magnetic effects in the highly charged Ca XVIII and Ti XX ions, the FS splittings are large in these systems compared to the Li atom. In Tables II to IV, we give the values of  $S$  and  $A$  from the E1, M1, and E2 channels from the excited states to the low-lying states of Li I, Ca XVIII, and Ti XX, respectively. Using these values, we have calculated the lifetimes of the excited states which are given in the same table. Our theoretical estimated lifetimes of the excited states in Li I are in good match with the experimental values [44–47]. Experimental results for the lifetimes of the excited states of Ca XVIII are not available. So, we compare the results with the previously reported theoretical results [48] (see Table III) and find reasonably good agreement between these results as well. In fact, there are neither any measurements nor any theoretical values of the lifetimes of the excited states in Ti XX are known. Nevertheless, we foresee similar levels of accuracies in these results, given in Table IV, based on the calculations in Li I and Ca XVIII.

After establishing the accuracies of various quantities of our interest in the isolated atomic systems, we now proceed in presenting these properties of the plasma embedded systems by considering finite values of  $D$  in Eq. (7). Unlike the isolated system, the IP of the plasma embedded system is no longer stable and it changes depending upon the strength of the plasma environment. As can be seen from Eq. (2) that  $D$  is a function of the plasma electron density ( $n_e$ ) and plasma temperature ( $T_e$ ). It is, therefore, possible to generate various plasma conditions by varying these parameters. For this purpose, we have varied the values of  $D$  from 0.5 to 200 a.u., 0.045 to 7.52 a.u., and 0.04 to 8.33 a.u. in the calculations of the above quantities in Li I, Ca XVIII and Ti XX, respectively. In Fig 1, we plot variation of the IPs of the ground states of Li I, Ca XVIII and Ti XX against the  $D$  values considering both Model A and Model B approximations. As expected, the IPs decrease with decrease in  $D$  values in both the models which is one of the unique characteristics of the plasma embedded atomic systems as referred as IPD or continuum lowering [9–12]. In Model A, the lower values of  $D$  around which the systems exist are 14 a.u., 0.3 a.u., and 0.25 a.u. in Li I, Ca XVIII and Ti XX, respectively, and below these critical values of  $D$ , the systems are supposed to be unbounded. After introducing the screenings in the repulsive interactions through Model B, the above critical values change from 14 a.u.

to 0.4 a.u., 0.3 a.u. to 0.043 a.u., 0.25 a.u. to 0.04 a.u., respectively, in Li I, Ca XVIII and Ti XX. It is evident from Fig. 1 that the IPs obtained in both the models are almost same for large  $D$  values but they differ for smaller values of  $D$  (large plasma couplings). To show it more prominently, we plot the differences of IPs from Model B and Model A ( $\Delta\text{IP} = \text{IP}_B - \text{IP}_A$ ) in Fig. 2 against the  $D$  values. It is obvious from this figure that  $\Delta\text{IP}$  shows slow variation for large  $D$  values while there are drastic differences and are positive for the smaller values of  $D$  (large screening). This indicates high stability of the systems in the presence of screening effects through the electron-electron repulsion.

We also plot the variations in EEs of the first six low-lying excited states of Li I, Ca XVIII and Ti XX against the  $D$  values in Figs. 3, 4, 5, respectively, for both Model A and Model B. First, we discuss the effects of plasma on EEs in the above systems using Model A. Fig. 3 shows that the EEs of the  $2p_{1/2,3/2}$ ,  $3p_{1/2,3/2}$ ,  $3d_{3/2,5/2}$ ,  $4s_{1/2}$ , and  $4p_{1/2}$  states in Li atom decrease with decrease in  $D$  values and finally, the states are merged into the continuum. Similar features are also observed in the highly charged Ca XVIII and Ti XX ions except for the  $2p$  states (see Figs. 4 and 5). In these states, the EEs of the  $2p$  states increase towards the strong screening strengths. Such signatures were also reported earlier in the H-like systems [49], He-like systems [50], and Li-like systems [51]. Therefore, Model A suggests that there are blue shifts in the  $2s-2p$  transitions in the plasma embedded Ca XVIII and Ti XX ions while all the EEs in Li I show red shifts for the reducing values of  $D$ . The figures also indicate that the embedded systems lose their capability to hold the bound states with increasing in plasma strengths and hence, possess only a finite number of energy levels as compared to their counter isolated ones.

Now coming to the EEs obtained from Model B, it is clear from Figs. 3, 4 and 5 that the EEs of all the states except for the  $2p$  states decrease with decreasing in  $D$  values. Thus, these transitions show red-shifts and finally, move to continuum at the critical values of  $D$ . The EEs of the  $2p$  states show different behavior; they are blue-shifted for larger the  $D$  values (smaller screening), and then gradually become red-shifted towards the smaller  $D$  region (higher screening). To realize these behaviors extensively, we plot the EEs of the  $2s - 2p_{1/2}$ ,  $2s - 3p_{1/2}$ ,  $3s - 3p_{1/2}$ , and  $3s - 4p_{1/2}$  transitions of Li I and Ca XVIII against the  $D$  values in Figs. 6 and ??, respectively, by considering Model B. It is clear from these figures that the EEs of the  $2s - 3p$  and  $3s - 4p$  transitions decrease with decrease in  $D$  values as per the findings in Model A [51]. However, the quantities for the  $2s - 2p$  and  $3s - 3p$  transitions increase initially with decreasing in  $D$  values and then fall suddenly in the lower  $D$  region. Similar trends are also observed in the Ti XX ion. We infer from this behavior that the  $\Delta n \neq 0$  transition spectra are red-shifted with decreasing in  $D$  values for both Model A and Model B, however the  $\Delta n = 0$  transition spectra are red-shifted in the Li atom and blue-shifted in the

Ca XVIII and Ti XX ions with decreasing  $D$  values for Model A. In contrast, the spectra for  $\Delta n = 0$  transitions show blue-shifts at the higher values of  $D$  and red-shifts for the lower values of  $D$  in all the atomic systems embedded in plasma when Model B is taken into account. This indicates that the effects of the two-electron screenings become less important for higher values of  $D$  (lower screening strengths) for which the results of Model A and Model B show nearly same behavior, but these screening effects play significant roles to influence the results at the lower values of  $D$  (higher screening strength) by producing a hump like structure. It is worth pointing out here that similar features have also been observed by Bowen *et al.* in the He-like systems [39].

Figs. 3, 4 and 5 also disclose that there appear to be changes in the energy level structures in the high screening regions with Model B with respect to the isolated systems. In Li I, it shows energy level crossings between the  $2p$  and  $3s$  states near to the continuum edge. The  $2p$  states move to continuum towards very lower  $D$  values whereas the  $3s$  state still exists there. Similar level crossings are also seen in the Li-like Ca and Ti ions near to the high screening regions. In the ionized systems, the level crossings become more obvious. To demonstrate these level-crossing processes in the plasma embedded systems, we give the Grotrian energy levels diagram, particularly in Ca XVIII, for few selective values of  $D$  in Fig. 8. This figure shows the change in the sequence of energy levels with the decreasing in values of  $D$ . For lower screening lengths, there found to be sequence alternative of the energy levels. As seen in this figure, the lower  $3d_{3/2,5/2}$  levels of Ca XVIII ion moved to the continuum around  $D = 0.3$  a.u. even when the  $4s_{1/2}$  state is still bounded with the ion. This implies that there are level crossings between the  $4s$  and  $3d$  states. There are also cross-overs among the  $4s$ ,  $3s$ ,  $2p$ , and  $3p$  states in this ion such as its energy level sequence becomes as  $2s$ ,  $3p_{1/2,3/2}$ ,  $2p_{1/2,3/2}$ ,  $3s$ , and  $4s$ . A similar trend is also noticed in the Li-like Ti ion. Fig. 8 also illustrates that the states with  $n = 3$  in Ca XVIII ion are nearly degenerate for the higher values of  $D$ , but the differences among the  $3s$ ,  $3p$  and  $3d$  states increase with the decreasing values of  $D$ . Gradually towards the high screening lengths, the cross-overs occur among the  $3s$ ,  $3p$  and  $3d$  energy levels, probably, owing to the weaker attraction of bound electrons by the nucleus. It is, however, found from Fig. 8 that the FS splittings between the states are least affected by the plasma screening. Indeed, we find that the states with larger orbital angular momentum are more affected by the screenings leading to the remarkable change in the energy level structures of the plasma embedded atomic systems near the continuum edge.

Since the energy spectra of the considered atomic systems are affected by the plasma environment, it is obvious that the radiative properties such as lifetimes of the excited states in these systems are different than their corresponding isolated systems. By calculating the line strengths for various allowed and forbidden transitions,

we evaluate the lifetimes of the excited states in the considered systems with different values of  $D$ . The variations in the lifetimes of the  $2p_{1/2}$ ,  $3s_{1/2}$ ,  $3p_{1/2}$ ,  $3d_{3/2}$  and  $4s_{1/2}$  states in Li I and Ca XVIII for different  $D$  values are listed in Table V. We plot them against the  $D$  values in Fig. 9 from which we found that the lifetimes of the  $2p$  states in Li I decrease slowly with increasing plasma strengths. Similar trends are also seen for the  $3p$  states in the Na atom by an earlier study [52]. Moreover, the lifetimes of the  $3s$ ,  $3d$ , and  $4s$  states show sharp rise in the high screening region.

The line intensity ratio of multiplet components in an atomic system is an important tool to determine various plasma parameters which are useful for both the laboratory and astrophysical plasma studies [53–56]. Under the local thermodynamic equilibrium (LTE), the line intensity ratio of plasma embedded atomic systems in the optically thin plasma is given by [57]

$$\frac{I_1}{I_2} = \left( \frac{\lambda_{nm}}{\lambda_{ki}} \right) \left( \frac{g_k A_{ki}}{g_n A_{nm}} \right) e^{-(E_k - E_n)/k_B T_e}, \quad (20)$$

where  $I_1$ ,  $I_2$  are the line intensities and  $\lambda_{ki}$ ,  $\lambda_{nm}$  are the wavelengths of the corresponding  $k \rightarrow i$  and  $n \rightarrow m$  transitions, respectively, of the atomic system. Here  $gA$ s are the weighted transition probabilities and  $E_k$ ,  $E_n$  are the energies of the respective upper  $k$  and  $n$  states, respectively.

The variation in the line intensity ratios between the ( $2p^2P_{1/2} - 3d^2D_{3/2}$ ) and ( $2p^2P_{3/2} - 3s^2S_{1/2}$ ) allowed transitions of Ca XVIII and Ti XX ions with respect to  $D$  for Model B are plotted in Fig. 10. The outer plot in Fig. 10 is for the Ca XVIII ion and the inset plot is given for the Ti XX ion. These calculations are carried out at  $T_e$  of 600 eV and 800 eV for Ca XVIII and Ti XX ions, respectively. It is evident from this figure that the variation in the intensity ratios of the above transitions increase rapidly with the  $D$  values. Similar features were also reported earlier in the H-like [49] and Be-like [58] systems. Our computed line intensities ratio between the above transitions with  $n_e = 2 \times 10^{21}$  and  $T_e = 600$  eV for Ca XVIII is coming out to be 9.42 against the observed value 7.8 [31]. Similarly, we obtain this value as 9.60 for Ti XX with  $n_e = 1 \times 10^{21}$  and  $T_e = 800$  eV compared to the experimental result 8.4 [31]. Although these results agree qualitatively, but the discrepancies between our estimated values from the observations can be the consequences of the approximations used in the Debye model for which we suggest consideration of more accurate theoretical calculations. One of the suitable approaches to minimize the differences in these results would be to include the exact form of the screening term in the two-body interaction potentials.

## V. CONCLUDING REMARKS

We have investigated the effects of plasma confinement on the electronic structure and spectroscopic properties

of the Li atom and highly charged Li-like Ca XVIII and Ti XX ions with two different approximations in the Debye model using a relativistic coupled-cluster method. The important findings from this work are summarized pointwise as follows:

1. In the presence of plasma confinement, the ionization potentials of the embedded systems decrease with decreasing in Debye lengths. Finally, at particular Debye length, the energy levels of the embedded systems merge into the continuum.
2. It is found that inclusion of the screening effects in the electron-nucleus interaction potentials destabilize the systems. In contrast, inclusion of the screenings in the electron-electron potentials counteract these effects by lowering the energies of the embedded systems, hence providing more stability to the systems.
3. With Model A approximation, all the transition spectra in the Li atom show red shifts with increasing in plasma strengths. But in case of Ca XVIII and Ti XX ions, the spectra corresponding to the  $ns - np$  transitions show blue shifts and the  $ns - n'p$  transitions exhibit red-shifts with increasing in plasma strengths. However, the systems display some peculiar behavior in the presence of screenings in the electron-electron interactions through Model B approach. It is found that the  $\Delta n \neq 0$  transition spectra of the plasma embedded systems are red shifted with increasing in plasma strengths and the feature is unchanged for both Model A and Model B. In case of Model B, the

$\Delta n = 0$  transitions show blue shifts at the higher screening lengths and red shifts for lower screening lengths due to the presence of the screenings in the electron-electron interactions.

4. In the presence of screening effects in both the electron-nucleus and the electron-electron interactions, the sequence of energy levels change for lower Debye lengths in comparison to the plasma isolated systems. The level-crossings between the states become more prominent in the highly ionized systems.
5. For higher screening lengths, the states with the same principal quantum number remain degenerate but the differences in the energy levels are widen for decreasing values of  $D$ .
6. Due to the strong influence of the screenings in the energy spectra of the embedded atomic systems, the lifetimes of the excited states change in comparison to their counter plasma free systems.

Our reported spectral properties will be useful in the studies of both the laboratory and astrophysical plasma for identifying the spectral lines in the considered atomic systems and will motivate the experimentalists to verify the theoretical findings.

#### Acknowledgments

This work has been supported by Council of Scientific and Industrial Research, India. A part of the computations were carried out using 3TFlop HPC cluster at Physical Research Laboratory, Ahmedabad.

- 
- [1] F. J. Rogers and C. A. Iglesias, *Science* **50**, 263 (1994).
  - [2] E. Storm, *Fusion J. Energy* **7**, 131 (1988).
  - [3] G. Mourou and D. Umstadter, *Phys. Fluids. B* **4**, 2315 (1992).
  - [4] J. Workman, M. Nantel, A. Maksimchuk, and D. Umstadter, *Appl. Phys. Lett.* **70**, 312 (1997).
  - [5] M. M. Murnane, H. C. Kapreyn, M. D. Rosen, and R. W. Falcone, *Science* **251**, 531 (1991).
  - [6] O. Renner, D. Salzmann, P. Sondhaus, A. Djanoui, E. Krousky, and E. Forster, *J. Phys. B: At. Mol. Opt. Phys.* **31**, 1379 (1998).
  - [7] A. Saemann, K. Eidmann, I.E. Golovkin, R.C. Mancini, E. Andersson, E. Forster, and K. Witte, *Phys. Rev. Lett.* **82**, 4843 (1999).
  - [8] M. S. Murillo and J. C. Weisheit, *Phys. Rep.* **302**, 1 (1998).
  - [9] D. R. Inglis and E. Teller, *Astrophys. J.* **90**, 439 (1939).
  - [10] R. P. Feynman, N. Metropolis, and E. Teller, *Phys. Rev.* **75**, 1561 (1949).
  - [11] G. Ecker and W. Kröll, *Phys. Fluids* **6**, 62 (1963).
  - [12] J. C. Stewart and K. D. Pyatt Jr., *Astrophys. J.* **144**, 1203 (1966).
  - [13] D. J. Hoarty, P. Allan, S. F. James, C. R. D. Brown, L. M. R. Hobbs, M. P. Hill, J. W. O. Harris, J. Morton, M. G. Brookes, R. Shepherd, J. Dunn, H. Chen, E. Von Marley, P. Beiersdorfer, H. K. Chung, R. W. Lee, G. Brown, and J. Emig, *Phys. Rev. Lett.* **110**, 265003 (2013).
  - [14] O. Ciricosta, S.M. Vinko, H.-K. Chung, B.-I. Cho, C.R.D. Brown, T. Burian, J. Chalupsky, K. Engelhorn, R.W. Falcone, C. Graves, V. Hajkova, A. Higginbotham, L. Juha, J. Krzywinski, H.J. Lee, M. Messerschmidt, C.D. Murphy, Y. Ping, D.S. Rackstraw, A. Scherz, W. Schlotter, S. Toleikis, J.J. Turner, L. Vysin, T. Wang, B. Wu, U. Zastra, D. Zhu, R.W. Lee, P. Heimann, B. Nagler, and J.S. Wark, *Phys. Rev. Lett.* **109**, 065002 (2012).
  - [15] Y. Y. Qi, J. G. Wang, and R. K. Janev, *Phys. Rev. A* **78**, 062511 (2008).
  - [16] B. Saha, P.K. Mukherjee, D. Bielinska-Waz, J. Karwowski, *J. Quant. Rad. Trans.* **92**, 1 (2005).
  - [17] S. Paul and Y. K. Ho, *Phys. Plasmas* **16**, 063302 (2009).
  - [18] J. K. Saha, S. Bhattacharyya, T. K. Mukherjee, and P. K. Mukherjee, *J. Phys. B: At. Mol. Opt. Phys.* **42**, 245701 (2009).
  - [19] C. Y. Lin and Y. K. Ho, *Phys. Rev. A* **81**, 033405 (2010).
  - [20] V. A. Boiko, A. V. Vinogradov, S. A. Pikuz, I. Yu. Sko-

- belev, and A. Ya. Faenov, X-ray Spectroscopy of Laser Produced Plasmas, *Itogi Nauki. Tekhniki Ser. Radio Engineering*, Moscow **27** VINITI (1980).
- [21] R. L. Kelly and L. J. Palumbo, NRL Report 7599. (U. S. Naval Research Laboratory, Washington, D. C., USA, 1973).
- [22] E. V. Aglitskii, V. A. Boiko, S. A. Pikuz, and A. Ya. Faenov, *Soviet Quant. Electronics* **1**, 1731 (1974).
- [23] E. Ya. Kononov, K. N. Koshelev, L. I. Podobedova, S. V. Chekalin, and S. S. Churilov, *J. Phys.* **B9**, 565 (1976).
- [24] G. E. Bromage, R. D. Cowan, B. C. Fawcett, H. Gordon, M. G. Hobby, N. J. Peacock, and A. Ridgeley, *Culham Lab. Report CLMR170* (1977).
- [25] P. G. Burkhalter, G. A. Doschek, and U. Feldman, *J. Opt. Soc. Am.* **67**, 741 (1977).
- [26] V. A. Boiko, A. Ya. Faenov, and S. A. Pikuz, *J. Quant. Spectrosc. Radiat. Transfer* **19**, 11 (1978).
- [27] B. C. Fawcett, A. Ridgeley, and T. P. Hyghes, *Mon. Nat. R. Astr. Soc.* **188**, 365 (1979).
- [28] V. A. Boiko, S. A. Pikuz, A. S. Safronova, and A. Ya. Faenov, *Phys. Scr.* **20**, 138 (1979).
- [29] G. Breton, C. DeMichelis, M. Finkenthal, and M. Mattioly, *J. Opt. Soc. Am.* **69**, 1652 (1979).
- [30] B. Edlen, *Phys. Scripta* **19**, 255 (1978).
- [31] J. C. Moreno, S. Goldsmith, and H. R. Griem, *J. Appl. Phys.* **65**, 1460 (1989).
- [32] W. Clark, M. Gersten, J. Katzenstein, J. Rauch, R. Richardson, and M. Wilkinson, *J. Appl. Phys.* **53**, 4099 (1982).
- [33] S. Djenize and J. Labat, *Bull. Astron. Belgrade* **154**, 17 (1996).
- [34] D. Ray and P. K. Mukherjee, *J. Phys. B: At. Mol. Opt. Phys.* **31**, 3479 (1998).
- [35] G. Hatton, N. F. Lane, and J. C. Weisheit, *J. Phys. B* **14**, 4879 (1981).
- [36] B. L. Whitten, N. F. Lane and J. C. Weisheit, *Phys. Rev. A* **29**, 945 (1984).
- [37] N.C. Deb and N. C. Sil, *J. Phys. B* **17**, 3587 (1984).
- [38] F. A. Gutierrez and J. Diaz-Valdes, *J. Phys. B* **27**, 593 (1994).
- [39] L. Bowen, D. Chenzhong, J. Jun, and W. Jianguo, *Plasma Sci. Technol.* **12**, 373 (2010).
- [40] Yashpal Singh, B. K. Sahoo, and B. P. Das, *Phys. Rev. A* **88**, 062504 (2013).
- [41] D. K. Nandy and B. K. Sahoo, *Phys. Rev. A* **88**, 052512 (2013).
- [42] D. K. Nandy, Yashpal Singh, B. P. Shah, and B. K. Sahoo, *Phys. Rev. A* **86**, 052517 (2012).
- [43] <http://physics.nist.gov/PhysRefData/ASD>.
- [44] D. Schulze-Hagenest, H. Harde, W. Brand, and W. Demtroder, *Z. Phys. A* **282**, 149 (1977).
- [45] U. Volz and H. Schmoranzner, *Phys. Scr. T65*, 48 (1996).
- [46] W. Nagourney, W. Happer, and A. Lurio, *Phys. Rev. A* **17**, 1394 (1978).
- [47] R. W. Boyd, J. G. Dodd, J. Krasinski, and C. R. Stroud, Jr., *Opt. Lett.* **5**, 117 (1980).
- [48] K. M. Aggarwal, F. P. Keenan, *At. Data and Nuc. Data Tables* **99**, 156 (2013).
- [49] Y. Y. Qi, J. G. Wang, and R. K. Janev, *Phys. Rev. A* **78**, 062511 (2008).
- [50] D. Ray and P. K. Mukherjee, *J. Phys. B* **31**, 3479 (1998).
- [51] Madhulita Das, Madhusmita Das, Rajat K. Chaudhuri, and Sudip Chattopadhyay, *Phys. Rev. A* **85**, 042506 (2012).
- [52] R. K. Chaudhuri, S. Chattopadhyay, and U. S. Mahapatra, *Phys. Plasmas* **19**, 082701 (2012).
- [53] F. P. Keenan, D. L. McKenzie, S. M. McCann, and A. E. Kingston, *Astrophys. J.* **318**, 926 (1987).
- [54] D. Porquet and J. Dubau, *Astron. Astrophys. (Suppl. Ser.)* **143**, 495 (2000).
- [55] T. Brage, P. G. Judge, and C. R. Proffitt, *Phys. Rev. Lett.* **89**, 281101 (2002).
- [56] D. G. Ellis, I. Martinson, and E. Träbert, *Comments At. Mol. Phys.* **22**, 241 (1990).
- [57] N. Konjevic and J. R. Roberts, *J. Phys. Chem. Ref. Data* **5**, 209 (1976).
- [58] B. Saha and S. Fritzsche, *Phys. Rev. E* **73**, 036405 (2006).

TABLE I: Comparison of our calculated ionization potentials (IPs), excitation energies (EEs) and fine-structure splittings (FS) in Li I, Ca XVIII and Ti XX with the national institute of science and technology (NIST) data [43] in  $cm^{-1}$ .

	Li		Ca XVIII		Ti XX	
	Present	NIST	Present	NIST	Present	NIST
	43482.67	43487.11	9340603.58	9337690	11499573.80	11495470
			IP			
			EE			
2p <sub>1/2</sub>	14909.23	14903.66	290372.20	290057	323898.05	323521
2p <sub>3/2</sub>	14909.19	14904	333108.78	330918	388627.13	385666
3s <sub>1/2</sub>	27202.15	27206.12	5259328.13	5276800	6468820.72	6465990
3p <sub>1/2</sub>	30923.83	30925.38	5339743.89	5338500	6558617.61	6555620
3p <sub>3/2</sub>	30923.81	30925.38	5352361.91	5350200	6577736.86	6574040
3d <sub>3/2</sub>	31277.94	31283.08	5382956.95	5381200	6612097.87	6608120
3d <sub>5/2</sub>	31277.95	31283.12	5386772.95	5384200	6617915.63	6613920
4s <sub>1/2</sub>	35007.66	35012.06	7063599.12	7059274.31	8691461.10	8687020
4p <sub>1/2</sub>	36466.32	36469.55	7096670.50	7112700	8728421.68	8724670
4p <sub>3/2</sub>	36466.31	36469.55	7101981.07	7118100	8736469.11	8732440
			FS			
2p <sub>1/2</sub> –2p <sub>3/2</sub>	0.04	0.34	42736.58	40861	64729.08	62145
3p <sub>1/2</sub> –3p <sub>3/2</sub>	0.02	0.0	12618.02	11700	19119.25	18420
3d <sub>3/2</sub> –3d <sub>5/2</sub>	0.01	0.04	3816.00	3000	5817.76	5800
4p <sub>1/2</sub> –4p <sub>3/2</sub>	0.01	0.0	5310.57	5400	8047.43	7770



TABLE II: Line strengths ( $S$ ), transition probabilities ( $A$ ) and lifetimes ( $\tau$  in  $ns$ ) of the excited states in Li atom. Numbers given in the square brackets represent powers of 10.

Transition $k \xrightarrow{O} i$	$S_{k \rightarrow i}$	$A_{k \rightarrow i}$	$\tau_k$	
			This work	Experiment
$2p_{1/2} \xrightarrow{E1} 2s_{1/2}$	11.019	3.70[7]	27.031	27.102 [44]
$2p_{3/2} \xrightarrow{E1} 2s_{1/2}$	22.024	3.70[7]	27.047	27.102 [44]
$2p_{3/2} \xrightarrow{M1} 2p_{1/2}$	1.33	6.05[-16]		
$3s_{1/2} \xrightarrow{M1} 2s_{1/2}$	8.1[-9]	2.21[-6]	29.82	29.72 [45]
$3s_{1/2} \xrightarrow{E1} 2p_{1/2}$	5.936	1.12[7]		
$3s_{1/2} \xrightarrow{E1} 2p_{3/2}$	11.877	2.24[7]		
$3p_{1/2} \xrightarrow{E1} 2s_{1/2}$	0.033	9.97[5]	210.82	203 [46]
$3p_{1/2} \xrightarrow{M1} 2p_{3/2}$	3.6[-8]	1.99[-6]		
$3p_{1/2} \xrightarrow{E2} 2p_{3/2}$	448.385	2.64[1]		
$3p_{1/2} \xrightarrow{E1} 3s_{1/2}$	71.746	3.75[6]		
$3p_{3/2} \xrightarrow{E1} 2s_{1/2}$	0.067	1.0[6]	210.62	
$3p_{3/2} \xrightarrow{M1} 2p_{1/2}$	3.2[-8]	8.80[-7]		
$3p_{3/2} \xrightarrow{E2} 2p_{1/2}$	448.410	1.32[1]		
$3p_{3/2} \xrightarrow{M1} 2p_{3/2}$	4.0[-10]	1.19[-8]		
$3p_{3/2} \xrightarrow{E2} 2p_{3/2}$	448.246	1.32[1]		
$3p_{3/2} \xrightarrow{E1} 3s_{1/2}$	143.484	3.75[6]		
$3d_{3/2} \xrightarrow{E2} 2s_{1/2}$	301.130	2.52[2]	14.58	14.60 [44]
$3d_{3/2} \xrightarrow{E1} 2p_{1/2}$	25.721	5.71[7]		
$3d_{3/2} \xrightarrow{E1} 2p_{3/2}$	5.145	1.14[7]		
$3d_{3/2} \xrightarrow{E2} 3s_{1/2}$	11.3[3]	3.56[-1]		
$3d_{3/2} \xrightarrow{E1} 3p_{1/2}$	136.954	3.08[3]		
$3d_{3/2} \xrightarrow{E1} 3p_{3/2}$	27.389	6.16[2]		
$3d_{5/2} \xrightarrow{E2} 2s_{1/2}$	451.743	2.52[2]	14.58	
$3d_{5/2} \xrightarrow{E1} 2p_{3/2}$	46.293	6.86[7]		
$3d_{5/2} \xrightarrow{E2} 3s_{1/2}$	16.9[3]	3.56[-1]		
$3d_{5/2} \xrightarrow{E1} 3p_{3/2}$	246.510	3.70[-1]		
$3d_{5/2} \xrightarrow{M1} 3d_{3/2}$	2.400	2.04[-18]		
$4s_{1/2} \xrightarrow{M1} 2s_{1/2}$	2.8[-8]	1.62[-4]	56.06	56 [47]
$4s_{1/2} \xrightarrow{E1} 2p_{1/2}$	0.420	3.46[6]		
$4s_{1/2} \xrightarrow{E1} 2p_{3/2}$	0.841	6.92[6]		
$4s_{1/2} \xrightarrow{E1} 3p_{1/2}$	36.042	2.49[6]		
$4s_{1/2} \xrightarrow{E1} 3p_{3/2}$	72.086	4.97[7]		
$4s_{1/2} \xrightarrow{E2} 3d_{3/2}$	8.5[3]	3.45[-1]		
$4s_{1/2} \xrightarrow{E2} 3d_{5/2}$	12.8[3]	5.17[-1]		

TABLE III: Line strengths ( $S$ ), transition probabilities ( $A$ ) and lifetimes ( $\tau$  in  $ps$ ) of the excited states in Ca XVIII ion. Numbers given in the square brackets represent powers of 10.

Transition $k \xrightarrow{O} i$	$S_{k \rightarrow i}$	$A_{k \rightarrow i}$	$\tau_k$	
			This work	Others [48]
$2p_{1/2} \xrightarrow{E1} 2s_{1/2}$	5.28[-2]	1.31[9]	763	753
$2p_{3/2} \xrightarrow{E1} 2s_{1/2}$	1.07[-1]	2.00[9]	501	504
$2p_{3/2} \xrightarrow{M1} 2p_{1/2}$	1.330	7.00[2]		
$2p_{3/2} \xrightarrow{E2} 2p_{1/2}$	6.35[-3]	2.54[-2]		
$3s_{1/2} \xrightarrow{M1} 2s_{1/2}$	1.04[-5]	2.04[4]	1.08	1.09
$3s_{1/2} \xrightarrow{E1} 2p_{1/2}$	2.42[-3]	3.01[11]		
$3s_{1/2} \xrightarrow{E1} 2p_{3/2}$	5.13[-3]	6.22[11]		
$3p_{1/2} \xrightarrow{E1} 2s_{1/2}$	1.52[-2]	2.35[12]	0.4258	0.4286
$3p_{1/2} \xrightarrow{M1} 2p_{1/2}$	8.39[-7]	1.46[3]		
$3p_{1/2} \xrightarrow{M1} 2p_{3/2}$	3.99[-5]	6.76[4]		
$3p_{1/2} \xrightarrow{E2} 2p_{3/2}$	4.78[-3]	8.42[8]		
$3p_{1/2} \xrightarrow{E1} 3s_{1/2}$	3.23[-1]	1.70[8]		
$3p_{3/2} \xrightarrow{E1} 2s_{1/2}$	2.96[-2]	2.30[12]	43.4	43.7
$3p_{3/2} \xrightarrow{M1} 2p_{1/2}$	1.39[-5]	1.22[4]		
$3p_{3/2} \xrightarrow{E2} 2p_{3/2}$	4.56[-3]	4.24[8]		
$3p_{3/2} \xrightarrow{M1} 2p_{3/2}$	3.25[-5]	2.77[4]		
$3p_{3/2} \xrightarrow{E2} 2p_{3/2}$	4.71[-3]	4.20[8]		
$3p_{3/2} \xrightarrow{E1} 3s_{1/2}$	6.49[-1]	2.65[8]		
$3p_{3/2} \xrightarrow{M1} 3p_{1/2}$	1.332	1.80[1]		
$3p_{3/2} \xrightarrow{E2} 3p_{1/2}$	2.35[-1]	2.11[-3]		
$3d_{3/2} \xrightarrow{E2} 2s_{1/2}$	1.52[-6]	1.60[3]	0.1432	0.1434
$3d_{3/2} \xrightarrow{E2} 2s_{1/2}$	1.74[-2]	2.20[9]		
$3d_{3/2} \xrightarrow{E1} 2p_{1/2}$	8.71[-2]	5.83[12]		
$3d_{3/2} \xrightarrow{E1} 2p_{3/2}$	1.77[-2]	1.16[12]		
$3d_{3/2} \xrightarrow{E2} 3s_{1/2}$	1.51[-1]	1.22[2]		
$3d_{3/2} \xrightarrow{M1} 3s_{1/2}$	4.01[-8]	5.11[-4]		
$3d_{3/2} \xrightarrow{E1} 3p_{1/2}$	4.18[-1]	1.71[7]		
$3d_{3/2} \xrightarrow{E1} 3p_{3/2}$	8.33[-2]	1.21[6]		
$3d_{5/2} \xrightarrow{E2} 2s_{1/2}$	2.61[-2]	2.21[9]	0.1432	0.1444
$3d_{5/2} \xrightarrow{E1} 2p_{3/2}$	1.59[-1]	6.93[12]		
$3d_{5/2} \xrightarrow{E2} 3s_{1/2}$	2.28[-1]	1.43[2]		
$3d_{5/2} \xrightarrow{E1} 3p_{3/2}$	7.52[-1]	1.03[7]		
$3d_{5/2} \xrightarrow{M1} 3d_{3/2}$	2.398	5.99[-1]		
$3d_{5/2} \xrightarrow{E2} 3d_{3/2}$	5.14[-2]	7.76[-7]		
$4s_{1/2} \xrightarrow{M1} 2s_{1/2}$	3.62[-6]	1.72[4]	1.607	1.612
$4s_{1/2} \xrightarrow{E1} 2p_{1/2}$	3.81[-4]	1.20[11]		
$4s_{1/2} \xrightarrow{E1} 2p_{3/2}$	7.98[-4]	2.47[11]		
$4s_{1/2} \xrightarrow{E1} 3p_{1/2}$	1.61[-2]	8.36[10]		
$4s_{1/2} \xrightarrow{E1} 3p_{3/2}$	3.39[-2]	1.72[11]		
$4s_{1/2} \xrightarrow{E2} 3d_{3/2}$	2.10[-2]	1.57[7]		
$4s_{1/2} \xrightarrow{E2} 3d_{5/2}$	3.18[-2]	2.36[7]		

TABLE IV: Line strengths ( $S$ ), transition probabilities ( $A$ ) and lifetimes ( $\tau$  in  $ps$ ) of the excited states in Ti XX ion. Numbers given in the square brackets represent powers of 10.

Transition $k \xrightarrow{O} i$	$S_{k \rightarrow i}$	$A_{k \rightarrow i}$	$\tau_k$ This work
$2p_{1/2} \xrightarrow{E1} 2s_{1/2}$	4.15[-2]	1.43[9]	700
$2p_{3/2} \xrightarrow{E1} 2s_{1/2}$	8.40[-1]	2.50[9]	500
$\xrightarrow{M1} 2p_{1/2}$	1.330	2.43[3]	
$\xrightarrow{E2} 2p_{1/2}$	4.17[-3]	1.33[-1]	
$3s_{1/2} \xrightarrow{M1} 2s_{1/2}$	3.33[-5]	1.22[5]	0.634
$\xrightarrow{E1} 2p_{1/2}$	2.19[-3]	5.14[11]	
$\xrightarrow{E1} 2p_{3/2}$	4.66[-3]	1.06[12]	
$3p_{1/2} \xrightarrow{E1} 2s_{1/2}$	1.31[-2]	3.74[12]	0.267
$\xrightarrow{M1} 2p_{1/2}$	1.27[-6]	4.15[3]	
$\xrightarrow{M1} 2p_{3/2}$	6.01[-5]	1.90[5]	
$\xrightarrow{E2} 2p_{3/2}$	3.16[-3]	1.58[9]	
$\xrightarrow{E1} 3s_{1/2}$	2.59[-1]	1.90[8]	
$3p_{3/2} \xrightarrow{E1} 2s_{1/2}$	2.54[-2]	3.66[12]	0.273
$\xrightarrow{M1} 2p_{1/2}$	2.10[-5]	3.47[4]	
$\xrightarrow{E2} 2p_{3/2}$	2.98[-3]	7.98[8]	
$\xrightarrow{M1} 2p_{3/2}$	4.89[-5]	7.82[4]	
$\xrightarrow{E2} 2p_{3/2}$	3.10[-3]	7.88[8]	
$\xrightarrow{E1} 3s_{1/2}$	5.21[-1]	3.41[8]	
$\xrightarrow{M1} 3p_{1/2}$	1.332	6.28[1]	
$\xrightarrow{E2} 3p_{1/2}$	1.54[-1]	1.10[-2]	
$3d_{3/2} \xrightarrow{E2} 2s_{1/2}$	2.48[-6]	4.85[3]	0.094
$\xrightarrow{E2} 2s_{1/2}$	1.16[-2]	4.09[9]	
$\xrightarrow{E1} 2p_{1/2}$	7.04[-2]	8.87[12]	
$\xrightarrow{E1} 2p_{3/2}$	1.43[-2]	1.75[12]	
$\xrightarrow{E2} 3s_{1/2}$	9.89[-2]	1.67[2]	
$\xrightarrow{E1} 3p_{1/2}$	3.38[-1]	2.62[7]	
$\xrightarrow{E1} 3p_{3/2}$	6.74[-2]	1.39[6]	
$3d_{5/2} \xrightarrow{E2} 2s_{1/2}$	1.73[-2]	4.12[9]	0.095
$\xrightarrow{E1} 2p_{3/2}$	1.29[-1]	1.06[13]	
$\xrightarrow{E2} 3s_{1/2}$	1.49[-1]	2.05[2]	
$\xrightarrow{E1} 3p_{3/2}$	6.09[-1]	1.33[7]	
$\xrightarrow{M1} 3d_{3/2}$	2.392	2.120	
$\xrightarrow{E2} 3d_{3/2}$	1.82[-2]	2.27[-6]	
$4s_{1/2} \xrightarrow{M1} 2s_{1/2}$	1.24[-5]	1.10[5]	1.35
$\xrightarrow{E1} 2p_{1/2}$	2.03[-4]	1.20[11]	
$\xrightarrow{E1} 2p_{3/2}$	4.32[-4]	2.51[11]	
$\xrightarrow{E1} 3p_{1/2}$	1.22[-2]	1.20[11]	
$\xrightarrow{E1} 3p_{3/2}$	2.59[-2]	2.48[11]	
$\xrightarrow{E2} 3d_{3/2}$	1.35[-2]	2.93[7]	
$\xrightarrow{E2} 3d_{5/2}$	2.05[-2]	4.40[7]	



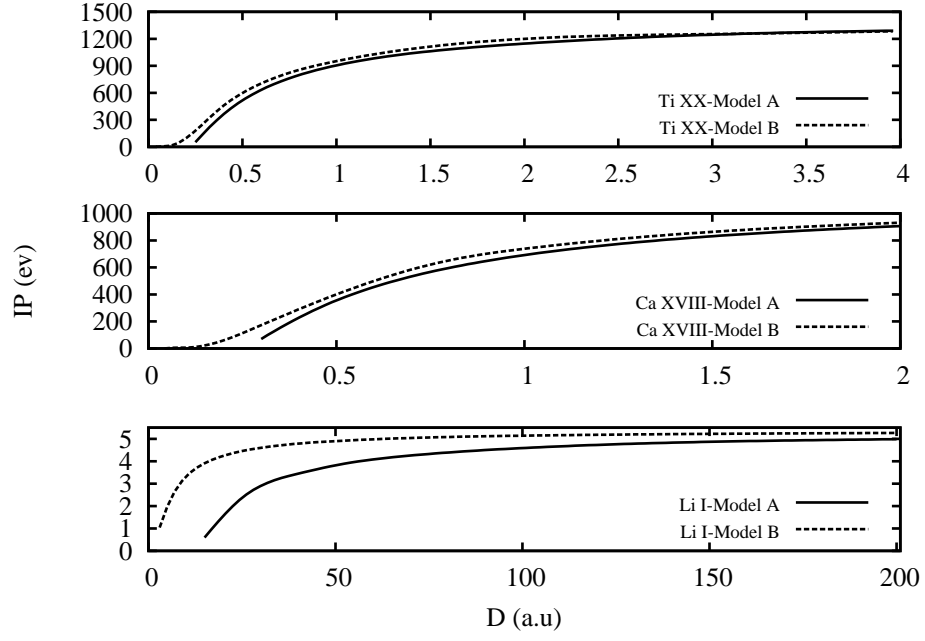


FIG. 1: Variation of ionization potentials with Debye screening length ( $D$ ).

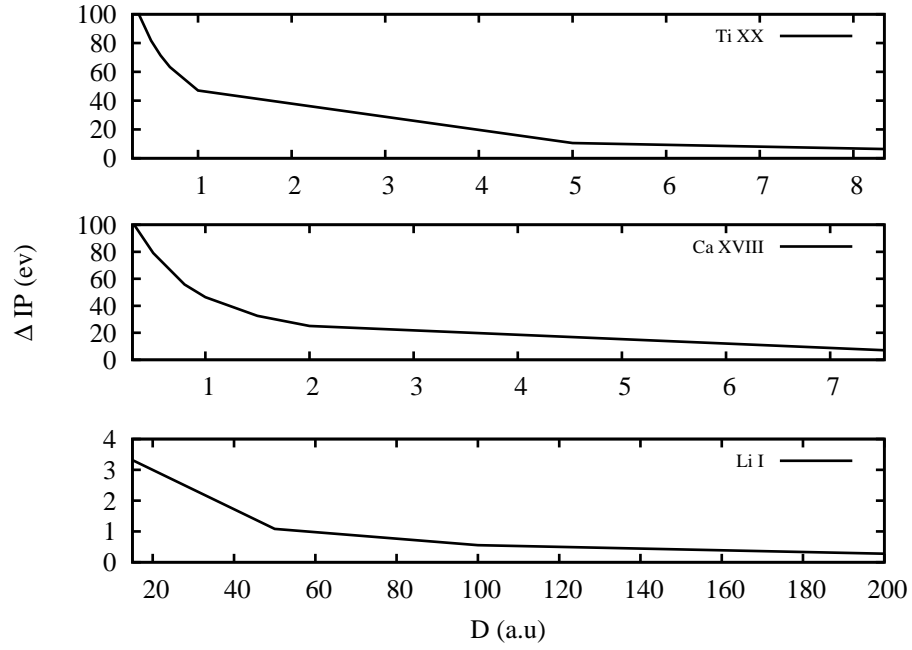


FIG. 2: Differences in the ionization potentials from Model B and Model A with Debye screening length ( $D$ ).

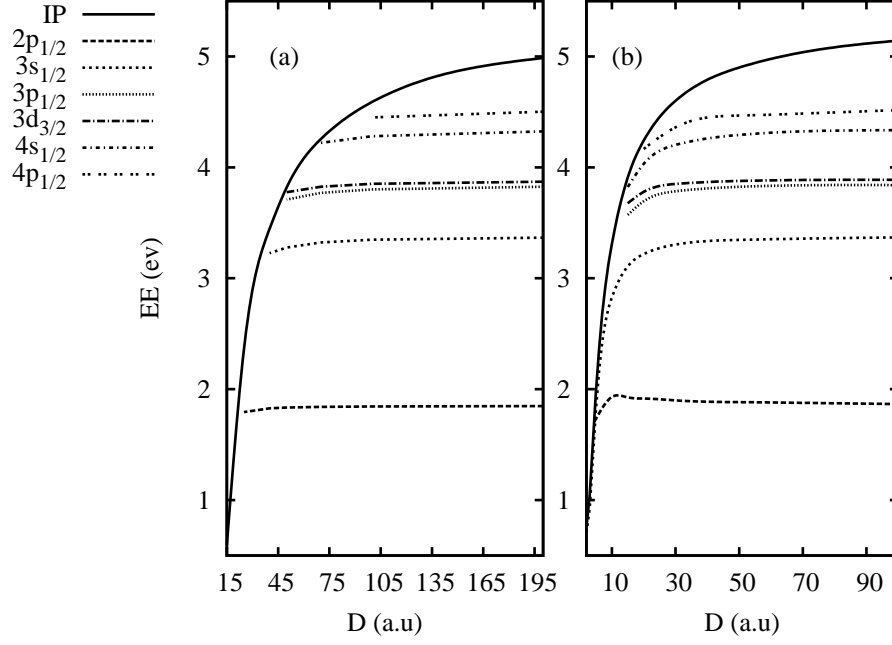


FIG. 3: Variation in the excitation energies of Li I with Debye screening length obtained from Model A shown in panel (a) and from Model B shown in panel (b).

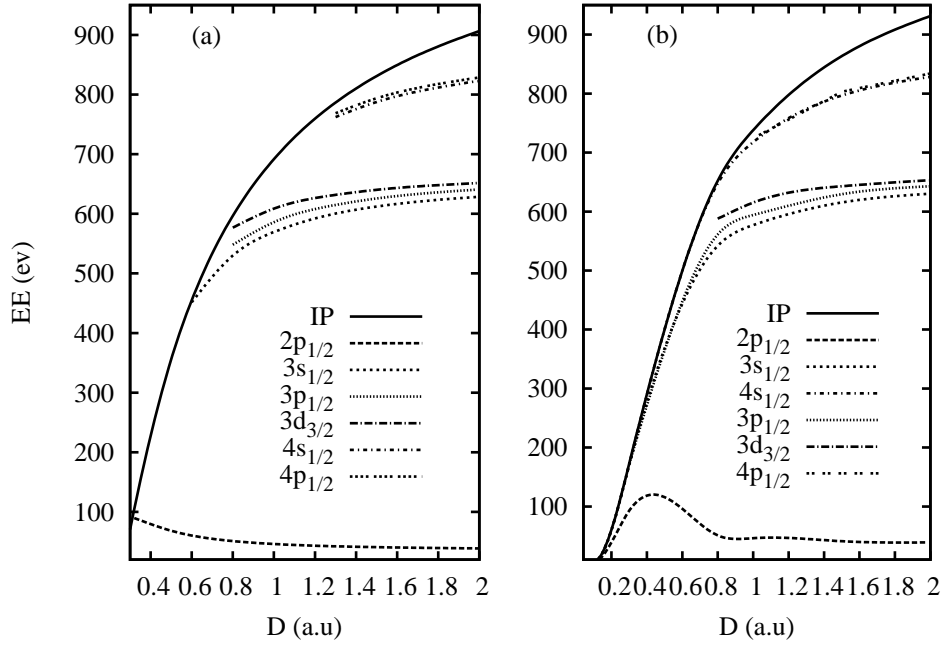


FIG. 4: Variation in the excitation energies of Ca XVIII with Debye screening length obtained from Model A shown in panel (a) and from Model B shown in panel (b).

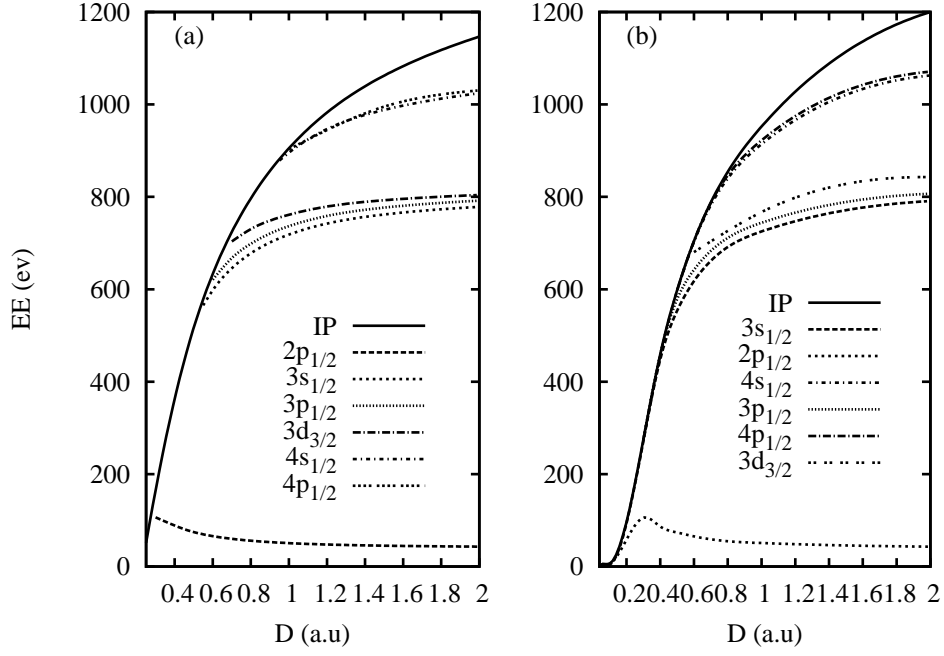


FIG. 5: Variation in the excitation energies of Ti XX with Debye screening length obtained from Model A shown in panel (a) and from Model B shown in panel (b).

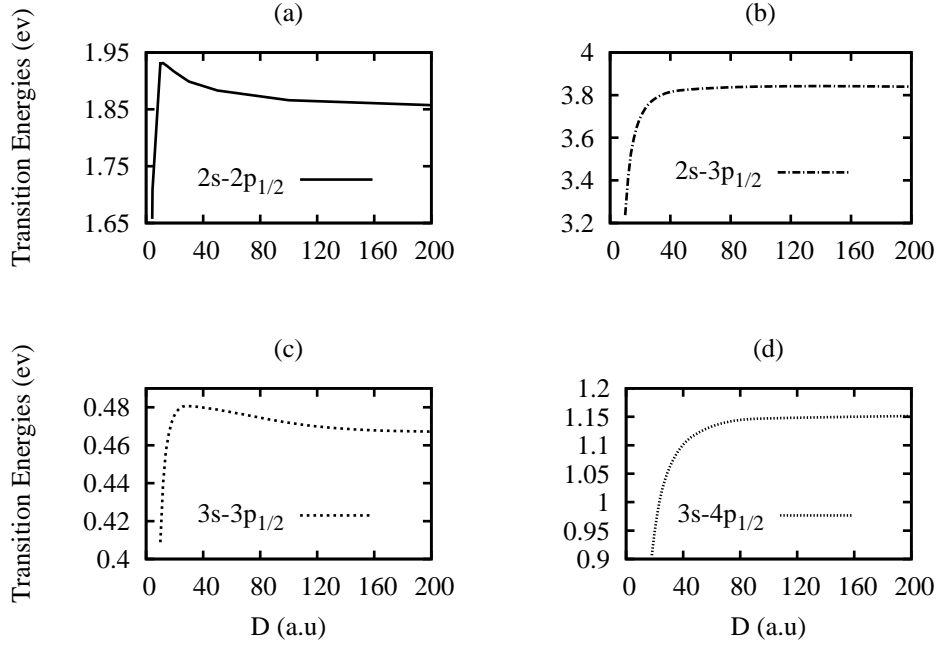


FIG. 6: Variation in the transition energies with Debye screening length in Li I using Model B. Panels (a) and (b) correspond to the  $2s_{1/2}$ - $2p_{1/2}$  and  $2s_{1/2}$ - $3p_{1/2}$  transitions, respectively, and panels (c) and (d) correspond to the  $3s_{1/2}$ - $3p_{1/2}$  and  $3s_{1/2}$ - $4p_{1/2}$  transitions, respectively.

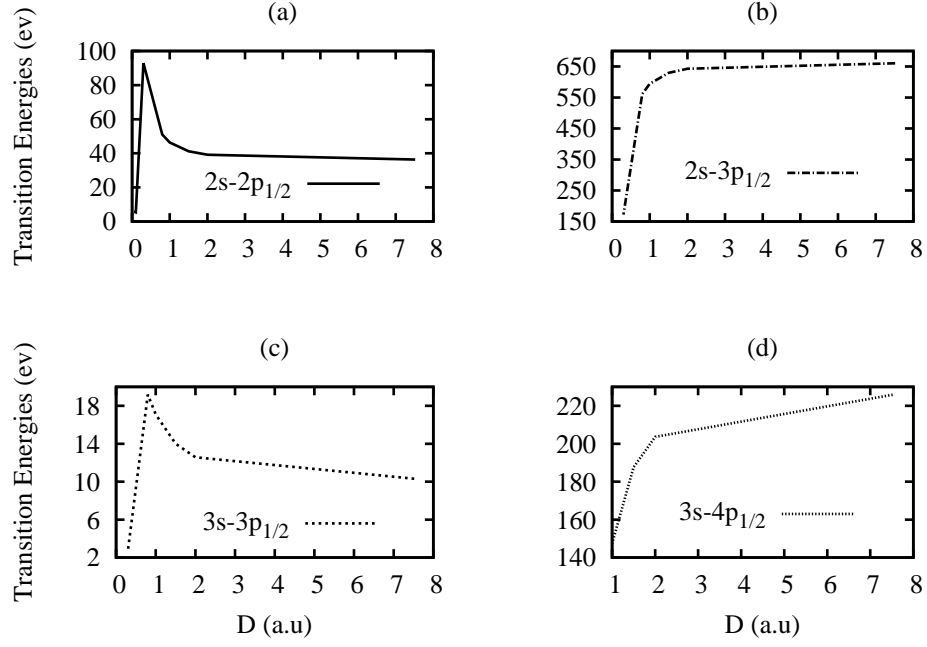


FIG. 7: Variation in the transition energies with Debye screening length in Ca XVIII using Model B. Panels (a) and (b) correspond to the  $2s_{1/2}-2p_{1/2}$  and  $2s_{1/2}-3p_{1/2}$  transitions, respectively, and panels (c) and (d) correspond to the  $3s_{1/2}-3p_{1/2}$  and  $3s_{1/2}-4p_{1/2}$  transitions, respectively.

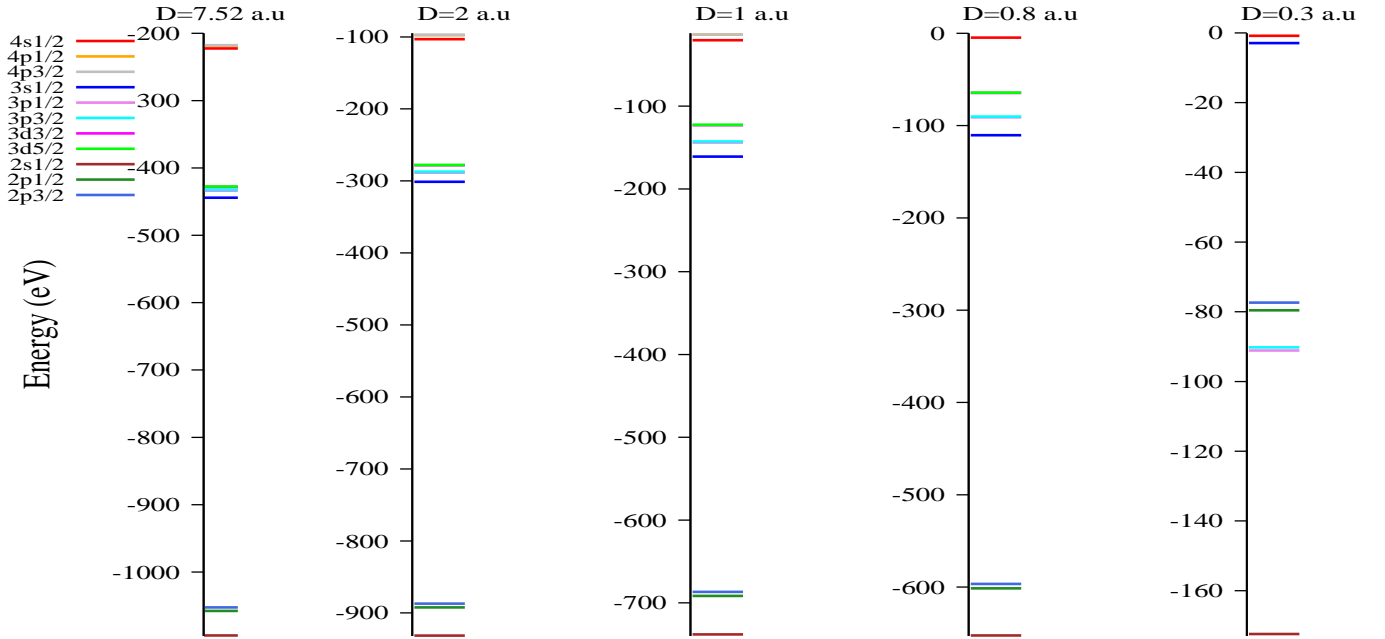


FIG. 8: (Color online) Grotrian diagram of energy levels in Ca XVIII for different values of  $D$  from Model B.

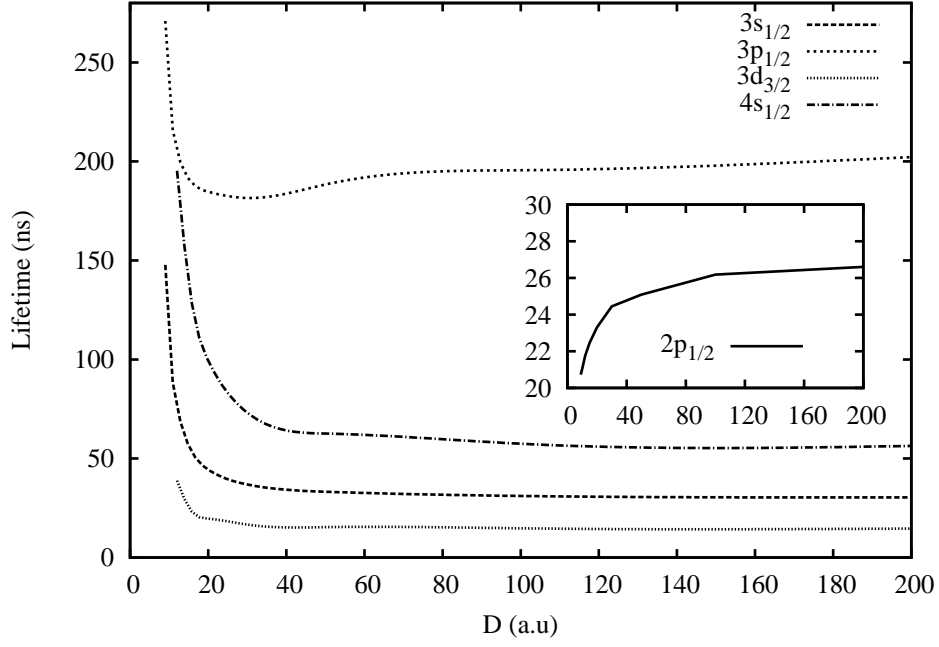


FIG. 9: Variation in the lifetimes of the excited  $3s_{1/2}$ ,  $3p_{1/2}$ ,  $3d_{3/2}$  and  $4s_{1/2}$  states in Li I with  $D$  values with Model B. The inset plot is for the  $2p_{1/2}$  state.

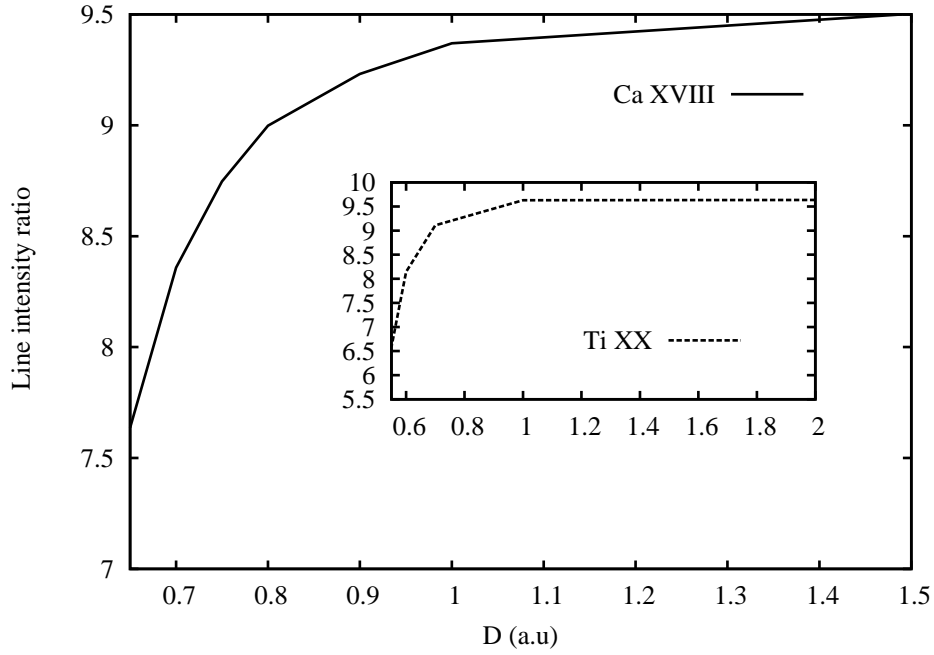


FIG. 10: Variation in the line intensity ratio of the  $3d^2 D_{3/2} \rightarrow 2p^2 P_{1/2}$  and  $3s^2 S_{1/2} \rightarrow 2p^2 P_{3/2}$  transitions of Ca XVIII with  $D$ . The same is shown in the inset plot for Ti XX.